Investigation on Contribution of Inductance Harmonics to Torque Production in Multiphase Doubly Salient Synchronous Reluctance Machines

K. Zhang, G. J. Li, Z. Q. Zhu, *Fellow, IEEE*, and G. W. Jewell

Department of Electronic and Electrical Engineering, University of Sheffield, Sheffield S1 4DE, U.K.

This paper investigates the contribution of each order inductance harmonic to the torque (both average torque and torque ripple) of multiphase doubly salient synchronous reluctance machines (DS-SRMs). Such machines are similar to switched reluctance machines but supplied with sine wave currents. The investigations in this paper are as follows. First, a general analytical torque model based on Fourier series analysis of inductances has been built for machines with different phase numbers, slot/pole number combinations, and also winding configurations. The instantaneous torque for DS-SRMs with any given phase number can then be accurately predicted. Using such model, contribution of each order inductance harmonic to torque can be investigated separately. It is found that the torque ripple frequency of the DS-SRM only depends on phase number. For example, for an m-phase machine, there will be m × kth-order torque ripple if mod(mk, 2) = 0, where m is the phase number and k is a natural number. This paper also explains why certain phase numbers inherently produce lower torque ripple than others. The findings in this paper provide a future direction for potential torque ripple reduction methods either from machine design or advanced control. The simulations have been validated by experiments using a six-phase DS-SRMs.

Index Terms— **Doubly salient, multiphase machine, synchronous reluctance machine, torque harmonic.**

I. Introduction

SWITCHED reluctance machines (SRMs) have excellent features such as simple and robust structures, high manufacturability, good fault-tolerant capability, and also low cost. In addition, without permanent magnets or field windings on the rotor, they are particularly suitable for harsh environmental operations such as high speed and high temperature. Due to these significant advantages, SRMs have attracted increasing interest in electric vehicles, aerospace, and other safety-critical applications [1], [2]. However, the doubly salient structure together with the special rectangular wave current supply causes high torque ripple, high vibrations, and acoustic noise compared with other types of machines. Therefore, in past decades, the torque ripple reduction is one of the most popular research topics for SRMs. This can be achieved from two aspects: machine design [3]–[5] and also advanced control [6], [7].

One effective and simple way to reduce the torque ripple is to increase the phase number. This method can be applicable not only to SRMs but also to synchronous (reluctance) machines and induction machines. Multiphase machines provide additional benefits apart from the torque ripple reduction because the machines with higher phase numbers ($m > 3$) can also have higher torque density and better fault-tolerant capability compared with conventional three-phase machines [8]. In addition, different winding configurations for multiphase machines can be selected to achieve even better torque performance [9], [10].

The conventional SRMs, with three-phase or multiphase, are supplied with rectangular wave current. However, recent studies have shown that they can be supplied with sine wave currents as well [11], [12]. It has been found that the sine wave excitations can bring benefit to the radial force reduction for SRMs, which are the primary source of vibrations and acoustic noise. One of the other advantages of sine wave excitation is that the standard three-phase voltage source inverter as that used in synchronous (reluctance) machines or induction machines can be employed, which can help reduce the system cost. It also provides a more flexible control strategy for SRMs to improve the torque performance. However, it is worth noting that the SRMs with sine wave current supply are actually doubly salient synchronous reluctance machines (DS-SRMs) [13]–[15].

Although the sine wave current supply has the above-mentioned advantages, it also brings some undesirable side effect, i.e., high torque ripple due to the nature of machine self- and mutual-inductances. To analyze the torque ripple mechanisms of different DS-SRMs, finite-element analysis (FEA) is often regarded as effective tools. However, they are more time-consuming and cannot really predict the contributions of each inductance harmonic to on-load torque. Other common analytical methods such as Maxwell stress tensor [16], [17], virtual work [18], [19], and Lorentz force law [20], [21] could be employed. However, due to the doubly salient structure, these methods become extremely complex and hard to implement.

To reduce the modeling complexity, a simple analytical torque model based on self- and mutual-inductances has been proposed for the investigated multiphase DS-SRMs. Although the inductances can be calculated according to winding function theories [18], [22], for simplicity they are calculated by

Manuscript received October 31, 2018; revised December 19, 2018 and January 30, 2019; accepted February 8, 2019. Date of publication March 5, 2019; date of current version March 18, 2019. Corresponding author: G. J. Li (e-mail: g.li@sheffield.ac.uk).

Color versions of one or more of the figures in this paper are available online at http://ieeexplore.ieee.org.

Digital Object Identifier 10.1109/TMAG.2019.2899803

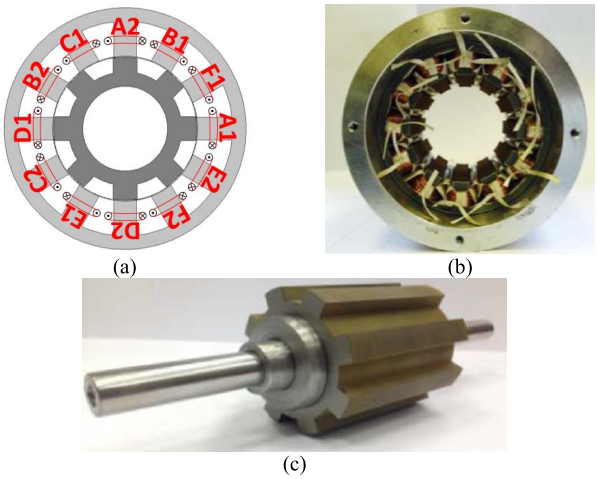

(a) (b) (c)

Fig. 1. (a) Cross section, (b) prototype 12-slot stator, and (c) 8-poles rotor for a DL 12s/8p six-phase DS-SRM.

TABLE I
MACHINE KEY DIMENSIONS AND DESIGN FEATURES

Stator outer radius (mm)	45
Split ratio	0.6
Air gap length (mm)	0.5
Active length (mm)	60
Number of turns per phase	132
Slot fill factor	0.37
Rated RMS current (A)	5

2-D-FEA in this paper. The proposed model can be applied for all kinds of DS-SRMs with different slot/pole combinations and wining configurations, e.g., double layer (DL), single layer (SL), and fully pitched (FP). Through harmonic analysis, the torque ripple frequency and magnitude for DS-SRMs with different phase numbers can be reliably predicted. In addition, the torque contribution due to each inductance harmonic can also be accurately quantified. As a result, the mechanism about why certain phase numbers can have inherently lower torque ripple, while others cannot, can be investigated. This will be helpful for researchers to find optimal measures in order to reduce torque ripple of DS-SRMs either from machine design or machine control perspectives.

II. SRM Analytical Torque Model

This paper covers DS-SRMs with various slot/pole combinations and different phase numbers, e.g., 4s/4p two phase, 6s/4p three phase, 8s/6p four phase, 10s/8p five phase, 12s/8p six phase, and 12/10p six phase. By way of example, Fig. 1 shows the cross section and prototype stator and rotor for DL 12s/8p six-phase DS-SRMs. The main specifications for all the topologies are listed in Table I. It is worth noting that the SL winding machines have the same key dimensions and also the same number of turns per phase as their DL counterparts. However, the number of turns per coil of SL machines will be doubled with the number of coils per phase being halved. In order to achieve optimal performance for multiphase DS-SRMs, the winding configurations have been designed according to the classic winding theory for synchronous machines (fractional slot and also integer slot) [23], [24].

According to the literature, the instantaneous torque equation of SRMs can be obtained based on the phase inductances

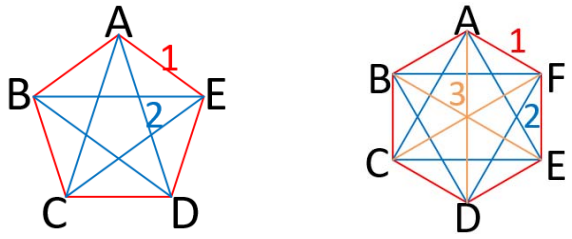

(a) (b)

Fig. 2. Relative phase order in space for (a) five-phase and (b) six-phase DS-SRMs.

(self and mutual) and phase currents [2], [3], [25]. Assuming the magnetic saturation can be neglected, the on-load torque of an m-phase SRM is given by

$$T_e = \frac{1}{2}[i_m]^T \frac{d[L_m]}{d\theta}[i_m] \tag{1}$$

where m represents the phase number, $[i_m] = [i_1, i_2, \ldots i_m]^T$. $[L_m]$ is an $m \times m$ inductance matrix. This equation can also be applicable for DS-SRMs and will be used to investigate the torque performance in this paper. The general current equation for phase x is written as

$$i_x = I_p \sin\left(\theta_e + \beta - \frac{2\pi}{m}(x-1)\right) \quad \text{with } x = 1, 2, \ldots m \tag{2}$$

where I_p is the amplitude of phase current, θ_e is the electric rotor position, and β is the current phase angle.

It is worth noting that for an m-phase DS-SRMs, the phase self-inductances have the same magnitude but have a $(2\pi/m)$ phase shift between them. However, the number of mutual inductances between phases is a function of phase number m, which can be calculated by $m \times (m-1)$. By way of example, Fig. 2(a) and (b) shows the relative phase order in space for five- and six-phase machines, respectively. The mutual inductances between two phases with the same distance in space will have the same waveform but with a $(2\pi/m)$ phase shift between them. The distance 1 means two phases are adjacent to each other, such as $M_{ab}, M_{bc}, \ldots$; the distance 2 means two phases are not adjacent and have an interval of one phase between them, such as $M_{ac}, M_{bd}, \ldots$ Similarly, the distance 3 has an interval of two phases as shown in Fig. 2(b), such as $M_{ad}, M_{be}, \ldots$ To be more generic, "Z" can be employed to express the number of different distances between phases for an m-phase DS-SRMs. It is the minimum integer not less than (C_m^2/m), as shown in the following equation:

$$Z \geq \frac{C_m^2}{m} = \frac{m!}{2!(m-2)! \times m} = \frac{m-1}{2}. \tag{3}$$

By way of example, for the 12s/8p DL six-phase DS-SRM, there are three types of mutual inductances due to $(C_6^2/6) = 2.5$. The inductance waveforms and their spectra are shown in Fig. 3.

In order to identify the contribution of inductance harmonics to the average torque and torque ripple, the self- and mutual-inductances are expressed using Fourier series analysis as

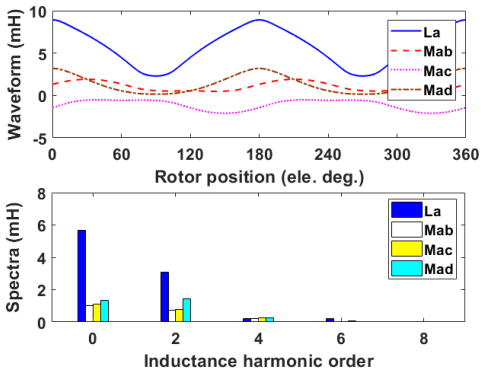

Fig. 3. Inductance waveforms and spectra of a DL six-phase DS-SRM. Calculated by FEA when phase A is supplied with a 1 A dc current.

shown in the following equations:

$$L = L_0 + \sum_{n=1}^{\infty} L_n \cos(n\theta_e + \alpha_n) \tag{4}$$

$$M_a = M_{a0} + \sum_{n=1}^{\infty} M_{an} \cos(n\theta_e + \alpha'_{an}) \tag{5}$$

where L and M_a represent the self- and mutual-inductances. α_n and α'_{an} are the phase angles of the nth self- and mutual-inductances, respectively. The subscript "0" represents the dc component of inductances. "a" represents the distance between two phases and $a \in (1, 2 \cdots Z)$. For example, M_{10} is the dc component of mutual inductance with the distance 1 in Fig. 2. Substituting (2), (4), and (5) into (1) gives

$$T_e = T_{\text{sel}} + T_{\text{mut}} \tag{6}$$

with

$$T_{\text{sel}} = \frac{mp}{2} \sum_{k=0}^{\infty} \left\{ -\frac{mk}{2} L_{mk} I_p^2 \sin(mk\theta_e + \alpha_{mk}) + \frac{mk-2}{4} I_p^2 L_{mk-2} \sin(mk\theta_e + 2\beta + \alpha_{mk-2}) + \frac{mk+2}{4} I_p^2 L_{mk+2} \sin(mk\theta_e - 2\beta + \alpha_{mk+2}) \right\} \tag{7}$$

and

$$T_{\text{mut}} = \frac{mp}{2} \sum_{k=0}^{\infty} \sum_{a=1}^{Z} c \left\{ -\frac{mk}{2} I_p^2 M_{amk} \sin\left(mk\theta_e + \alpha'_{amk}\right) + \frac{mk-2}{2} I_p^2 M_{a(mk-2)} \times \sin\left(mk\theta_e + 2\beta + \alpha'_{a(mk-2)} - \frac{2\pi}{m}a\right) + \frac{mk+2}{2} I_p^2 M_{a(mk+2)} \times \sin\left(mk\theta_e - 2\beta + \alpha'_{a(mk+2)} + \frac{2\pi}{m}a\right) \right\} \tag{8}$$

TABLE II
ACTIVE INDUCTANCE HARMONICS FOR CERTAIN ORDER TORQUE HARMONICS

m \ k		1	2	3
2	Torque	mk=2nd	mk=4th	mk=6th
	Inductance	2nd, 4th	2nd, 4th, 6th	4th, 6th, 8th
3	Torque	mk=3rd	mk=6th	mk=9th
	Inductance	1st, 3rd, 5th	4th, 6th, 8th	7th ,9th, 11th
4	Torque	mk=4th	mk=8th	mk=12th
	Inductance	2nd, 4th, 6th	6th, 8th, 10th	10th, 12th, 14th
5	Torque	mk=5th	mk=10th	mk=15th
	Inductance	3rd, 5th, 7th	8th, 10th, 12th	13th, 15th, 17th
6	Torque	mk=6th	mk=12th	mk=18th
	Inductance	4th, 6th, 8th	10th, 12th, 14th	16th, 18th, 20th

with

$$c = \begin{cases} 0.5 & \text{mod}(m,2) = 0 \text{ and } a = Z \\ 1 & \text{otherwise} \end{cases} \tag{9}$$

where T_{sel} and T_{mut} are the torques produced by the self- and mutual-inductances, respectively. p is the pole-pair number and k is a natural number. It can be seen that the average torque can be obtained when k is equal to "0." Moreover, only the interaction between fundamental current and second-order harmonic inductance can produce the average torque, which can be rewritten as

$$T_0 = \frac{mp}{4} I_1^2 L_2 \sin(-2\beta + \alpha_2) + \frac{mp}{2} \sum_{a=1}^{Z} c I_1^2 M_{a2} \sin\left(-2\beta + \alpha'_{a2} + \frac{2\pi}{m}a\right). \tag{10}$$

According to (6)–(8), it can be proven that for m-phase DS-SRMs, in general, there will be mkth-order torque harmonics when sine wave current is supplied. This is due to the interaction between the fundamental current and the mkth, $(mk \pm 2)$th-order inductance harmonics. The contributions of each order inductance harmonic to the torque ripple harmonic are listed in Table II. It is worth noting that from the above conclusion, the three-phase machine will in theory produce triplen order torque harmonics. However, due to the fact that the odd order inductances are equal to zero, therefore, the odd order torque harmonics, such as 3rd, 9th, and 15th, do not exist. This is the same for the five-phase machine, in which the 5th-, 15th-, 25th-…order torque harmonics do not exist. Moreover, it can be predicted that the two-phase and four-phase machines present the worst performance in terms of torque ripple when sine wave current is supplied. The reason is that all orders of inductance harmonics will contribute to the torque ripple for both types of machine. Even the second-order inductance (with the highest magnitude, and normally contributes to average torque) will produce the second- and fourth-order torque harmonics for the second-phase machine while produce the fourth-order torque harmonic for the four-phase machine. This can explain why certain phase numbers generate higher torque ripple, while others do not.

Fig. 4 shows the comparison results between 2-D-FEA and analytical prediction for a DL 12s/8p six-phase DS-SRM

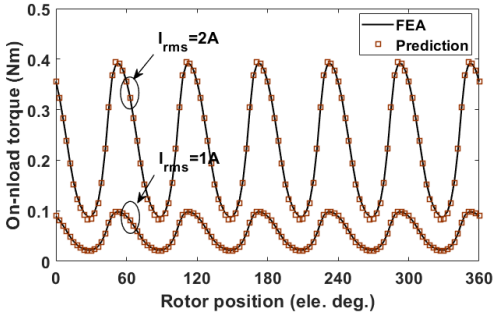

Fig. 4. Comparison of on-load torques between 2-D-FEA and analytical prediction for a DL 12s/8p six-phase DS-SRM at $I_{\rm rms} = 1$ and 2 A.

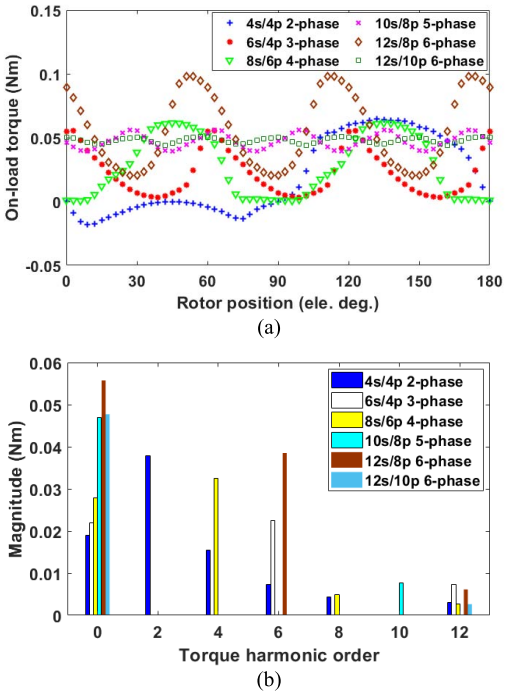

Fig. 5. Predicted results. (a) Instantaneous torque and (b) torque spectra for m-phase DL DS-SRMs. The machine is supplied with 1 A rms current.

at 1 and 2 A phase root-mean-square (rms) current. A generally good agreement can be observed, which validates the accuracy of the proposed analytical torque model. Therefore, only the prediction results of instantaneous torques and spectra are presented for other topologies, as shown in Figs. 5 and 6, respectively. As expected, the on-load torque of m-phase machines will contain the mkth torque order harmonic if $\mathrm{mod}(mk, 2) = 0$ is valid. However, it is worth noting that for the 12s/10p DL six-phase machine, the sixth ($k = 1$)-order torque ripple can be ignored, which is different from other types of six-phase machine. This will be investigated further in Section III.

III. Comparison Study of Six-Phase Topologies

This section will further investigate the influence of machine topologies and winding configurations on torque ripple of the six-phase machines. Several six-phase machines

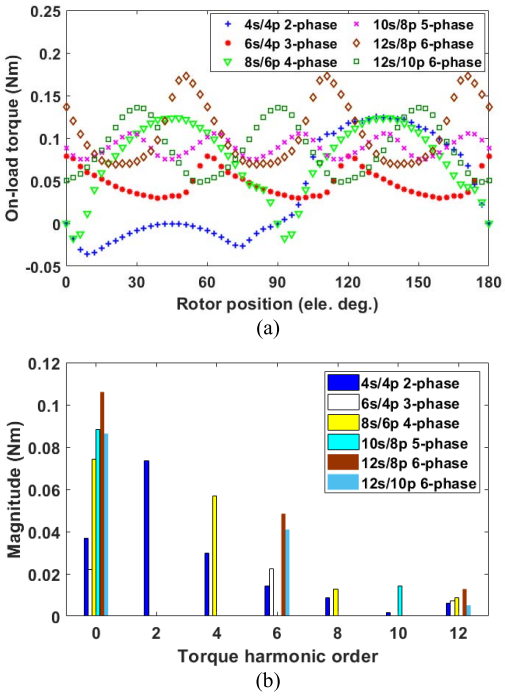

Fig. 6. Predicted results. (a) Instantaneous torque and (b) torque spectra for m-phase SL DS-SRMs. The machine is supplied with 1 A rms current.

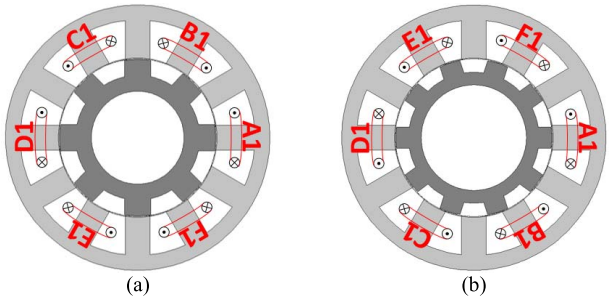

Fig. 7. Two types of six-phase SL DS-SRMs. (a) 12s/8p. (b) 12s/10p.

(12s/4p, 12s/8p, and 12s/10p) with different winding configurations (concentrated and distributed winding) have been considered.

A. Short-Pitched Concentrated Winding

By way of example, the two SL 12s/8p and 12s/10p six-phase DS-SRMs have been shown in Fig. 7.

According to (6)–(8), the comparison in terms of instantaneous torque and torque spectra for the four types of machines is given in Fig. 8. For different slot/pole number combinations of six-phase machines, the 6th, 12th-, 18th-…order torque harmonics will always exist. However, it is obvious from Fig. 8 that the sixth-order torque harmonic for the 12s/10p DL machine can be neglected, which is different from other six-phase machines. In order to figure out the reason behind, the 12s/8p and 12s/10p DL machines have been further studied. The inductance spectra are shown in Fig. 9. It can be seen that for the two topologies, their inductance harmonic magnitudes have little difference, but the phase angles are significantly different. This will dramatically influence the

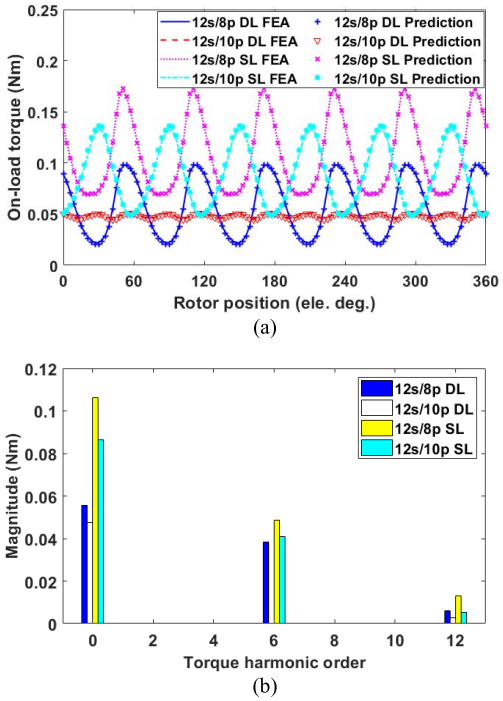

Fig. 8. Comparison of (a) on-load torque and (b) spectra for six-phase DS-SRMs. The machines are all supplied with 1 A rms current.

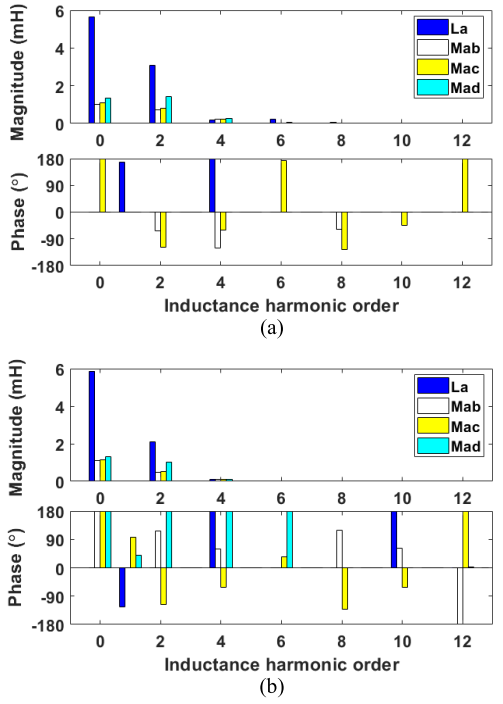

Fig. 9. Magnitudes and phases of inductance harmonics for (a) 12s/8p DL and (b) 12s/10p DL DS-SRMs.

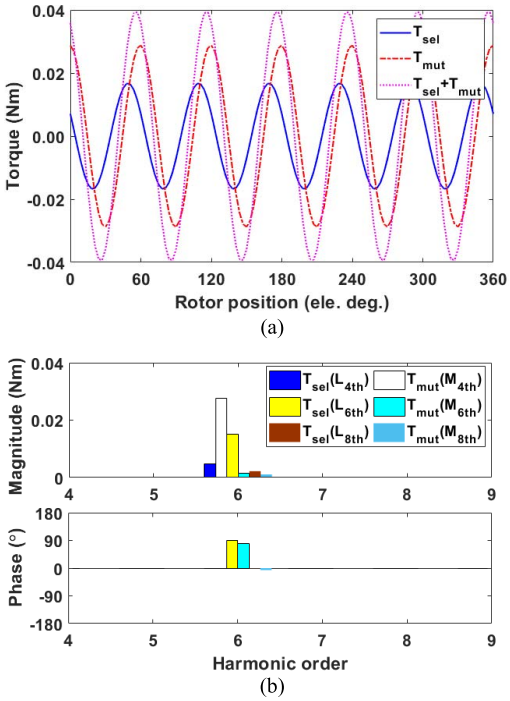

Fig. 10. Sixth-order torque harmonics of the 12s/8p DL DS-SRMs. (a) Resultant torque. (b) Self- and mutual-torques due to each inductance harmonic. The phase rms current is 1 A.

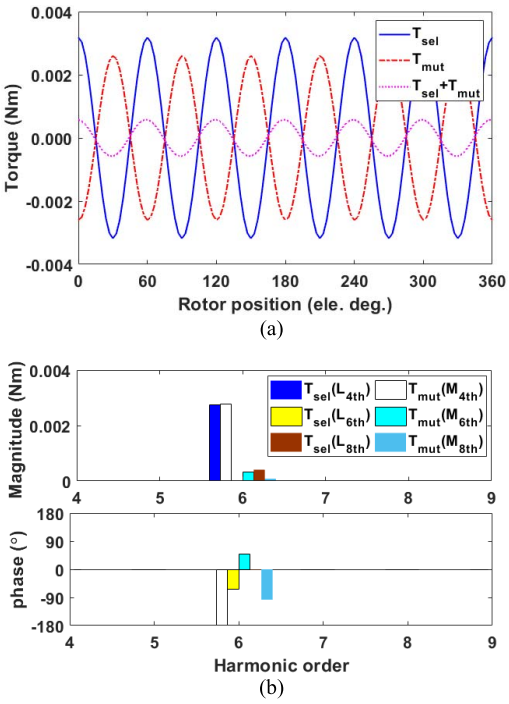

Fig. 11. Sixth-order torque harmonics of the 12s/10p DL DS-SRMs. (a) Resultant torque. (b) Self- and mutual-torques due to each inductance harmonic. The phase rms current is 1 A.

torque contribution of each inductance harmonic. The torque produced by each inductance harmonic can be predicted by using the proposed torque models (6)–(8), and the results are shown in Figs. 10 and 11.

From Figs. 10 and 11, it can be observed that the 12s/8p machine has much higher magnitudes in torque harmonics for every inductance harmonic than that of the 12s/10p. Moreover, for the 12s/8p machine, the self- and mutual-torques produced by the inductance harmonics have similar phase angles. As a result, the sixth-order torque harmonics due to the self- and mutual-inductances are additive, leading

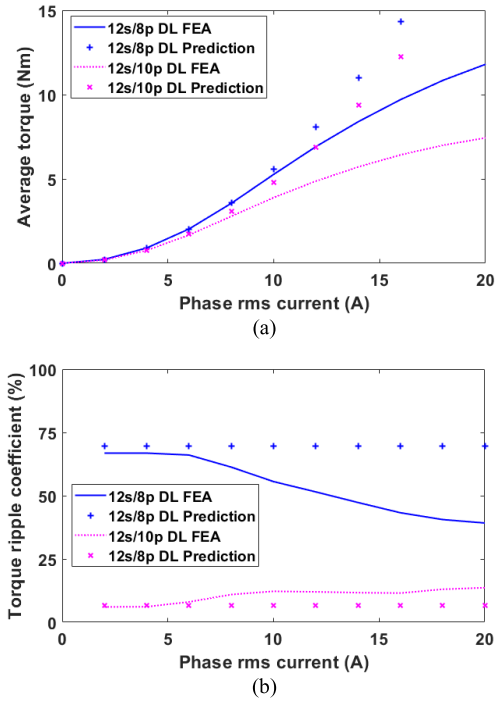

Fig. 12. Comparison of torque production for two topologies. (a) Average torque. (b) Torque ripple coefficient.

to higher overall torque ripple level. In contrast, the self- and mutual-torques of the 12s/10p machine have almost 180 elec. deg. phase difference. This is particularly the case for the self- and mutual-torques due to the fourth-order inductance harmonics. As a result, the sixth-order torque harmonics for the DL six-phase 12s/10p DS-SRMs cancel one another, leading to much lower overall torque ripple level.

It is worth noting that the proposed torque model is based on the phase inductances calculated at low electric loading. With the increasing phase current, the machines become saturated and there is an increasing discrepancy between the results obtained by FEA and the analytical torque models. The average torque and torque ripple coefficient $[(T_{\max} - T_{\min})/(2T_{\text{ave}}) \times 100\%$, where $T_{\max}, T_{\min}$, and T_{ave} are the maximum, minimum, and average torques for one electrical period] versus phase rms current, are shown in Fig. 12. It shows that the torque ripple benefit of the 12s/10p machine is not compromised at high saturation level compared with the 12s/8p machine.

B. Fully Pitched Distributed Winding

For completeness, apart from the concentrated winding configurations, six-phase FP DS-SRMs with distributed windings have also been investigated in this paper. Their cross sections and winding configurations are shown in Fig. 13. It is worth noting that the SL 12s/4p FP DS-SRMs have exactly the same torque performance as its DL counterpart. However, the DL winding does not work for the 12s/8p FP machines due to negligible torque capabilities. This is because the coil magnetomotive forces of each two opposite phases, e.g., phases A and D, have exactly the same polarity

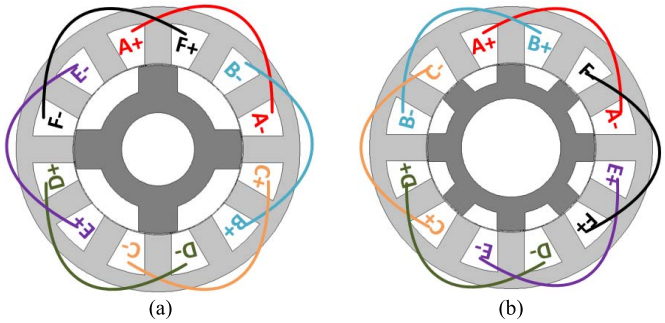

Fig. 13. Six-phase FP DS-SRMs. (a) 12s/4p. (b) 12s/8p.

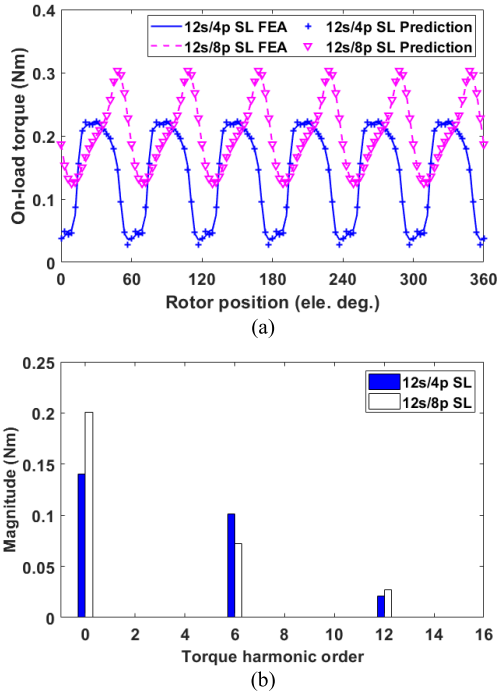

Fig. 14. Comparison of (a) torque and (b) FEA torque spectra for FP six-phase DS-SRMs with 1 A rms phase current.

(NN for phase A and NN for phase D as well) at each rotor position, there will be no return path for the armature flux. As a result, the air-gap flux density is almost zero, leading to very low output torque. Therefore, only SL winding topologies have been selected for investigation in this section.

The same analyses as in Section II have been performed for these two machines and the comparison results are shown in Fig. 14. Again, the proposed torque model provides reliable prediction in terms of on-load torque and there are 6th-, 12th-, and 18th-order torque harmonics as expected.

After comparative studies of different phase numbers, slot/pole number combinations, and also winding configurations, one can confirm that for any m-phase DS-SRMs, the torque harmonics due to fundamental current only depend on the phase number "m" and their orders are equal to mk when $\text{mod}(mk, 2) = 0$. However, without quantifying the contribution of each order inductance harmonic (magnitude) to torque, it is hard to identify which torque harmonic is the most dominant one.

TABLE III
PHASE RESISTANCES ACCOUNTING FOR END-WINDINGS FOR DIFFERENT TOPOLOGIES AT 20 °C

slot/pole	Phase number	DL (Ω)	SL (Ω)	FP (Ω)
4s/4p	2	0.638	0.789	-
6s/4p	3	0.766	0.893	-
8s/6p	4	0.993	1.111	-
10s/8p	5	0.985	1.089	-
12s/8p	6	1.02	1.116	1.617
12s/10p	6	1.02	1.116	-
12s/4p	6	-	-	1.617

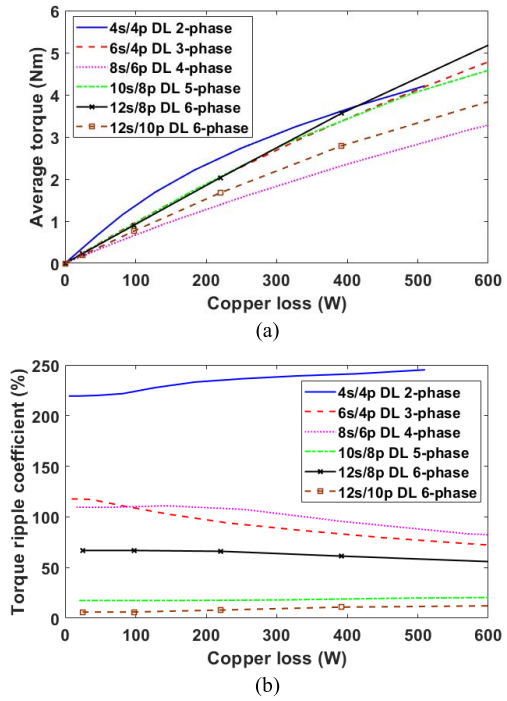

Fig. 15. (a) Average torque and (b) torque ripple coefficient versus copper loss for DL multiphase machines.

IV. COPPER LOSS FOR MULTIPHASE MACHINE

The investigated machines all have the same number of turns per phase so as to maintain similar phase voltage level. This means that for the same phase current, the copper losses will be different for different phase numbers. To be specific, higher phase number will have higher copper loss ($P_{\text{copper}} = mI^2R$, where R is the phase resistance and I is the phase rms current). In order to achieve fairer comparison, the average torque and torque ripple coefficient versus copper loss have been investigated in this section.

The phase resistances for different m-phase machines are listed in Table III. Here, different end-winding lengths have been considered, which can be calculated by using the method given in [26].

Figs. 15 and 16 show the average torque and torque ripple coefficient versus copper loss for the DL and SL DS-SRMs, respectively. It is found that for both DL and SL winding structures, the two-phase machines produce higher average torque than other phase numbers at low copper loss. With increasing phase current (or copper loss), the two-phase machines loss

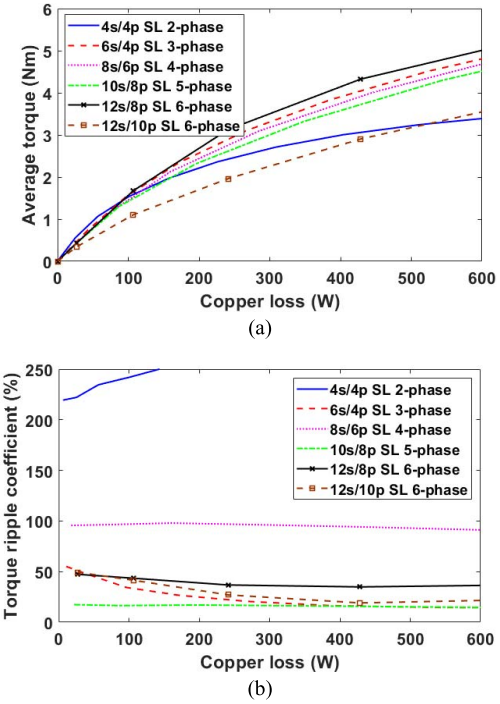

Fig. 16. (a) Average torque and (b) torque ripple coefficient versus copper loss for SL multiphase machines.

their benefit in terms of average torque, while the 12s/8p six-phase DS-SRMs will produce the highest average torque at higher copper loss (>400 W). Five-phase machines show similar torque capability as the 12s/8p six-phase machine at lower copper loss, while they have almost the smallest torque ripple coefficient compared with other machines expect the 12s/10p DL six-phase machine. In addition, the benefit in terms of torque ripple for the five-phase machine will not be compromised with increased copper loss. It is also worth noting that the DL/SL two-phase and four-phase DS-SRMs have shown much worse torque ripple performance, as expected.

The 12s/8p DL/SL six-phase machines have also been compared with two types of FP machines and the results are shown in Fig. 17. It shows when the copper loss is less than 600 W, the DL machines exhibit the lowest average torque compared with other three machines. When the phase current increases, so does the copper loss, the benefit of DL machines is increasing evidently. It is because they are less sensitive to magnetic saturation due to less flux concentrated in the stator yoke [26]. It is also apparent that the two FP machines show similar torque capability. However, the 12s/8p FP machines always achieve the lowest torque ripple compared with other machines, while the 12s/4p FP machines being the highest. Moreover, it is worth noting that the torque ripple of SL machines is generally lower than that of DL machines for lower current (copper loss < 1600 W). However, with increasing phase current, this advantage diminishes.

V. EXPERIMENTAL VALIDATION

A. Prototypes of SRMs

In order to validate torque capability of proposed six-phase DL and SL DS-SRMs (12s/8p), two prototype DS-SRMs

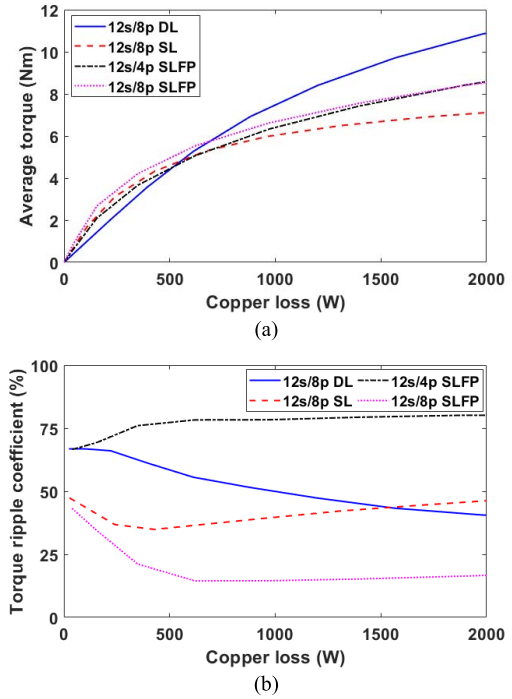

Fig. 17. (a) Average torque and (b) torque ripple coefficient versus copper loss for six-phase topologies.

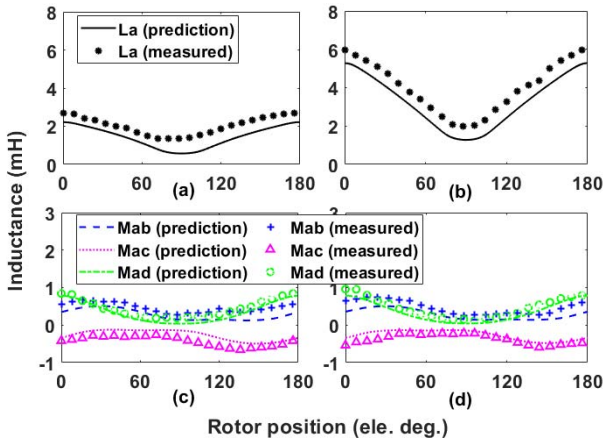

Fig. 18. FEA and measured self-inductance (L_a) and mutual-inductances with different distances (M_{ab}, M_{ac}, and M_{ad}) for 12s/8p six-phase DS-SRMs when phase A is supplied with a 2 A dc current. (a) and (c) DL. (b) and (d) SL.

with SL and DL windings, which were designed in [26], have been tested as six-phase models. It is worth noting that all m-phase SRMs in Sections II and III have the same number of turns per phase (132). However, due to the fact that the tested six-phase machines are converted from three-phase machines, the number of turns per phase is reduced by half (66). This means that the inductance will be reduced by four times, as shown in Fig. 18. The method of inductance measurement has been introduced in [27]. To be consistent with the prototype machines, the number of turns per phase in the FEA models in this section is also reduced to 66.

B. Self- and Mutual-Torque

The method of static torque measurement is detailed in [28] which will be applied to all torque measurement except

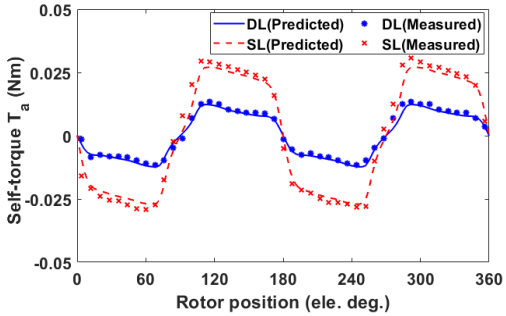

Fig. 19. FEA and measured resultant self-torques T_a for 12s/8p six-phase DS-SRMs when phase A is supplied with a 2 A dc current.

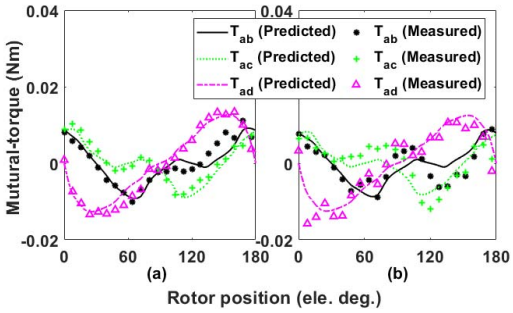

Fig. 20. FEA and measured mutual-torques with different distances for 12s/8p six-phase DS-SRMs when phase A is supplied with a 2 A dc current. (a) DL. (b) SL.

the on-load static torque in Section V-D. The stator is fixed on the lathe and can be rotated to change the relative angle between rotor and stator, i.e., rotor position, while the rotor shaft is connected with a balance beam and therefore cannot be rotated. There will be pre-load weight at the end of the beam to make sure it has a stable contact with the digital scale. After reading the mass at the end of beam by digital scale, the torque at a fixed rotor position can be calculated by $T_e = (m_r - m_{\text{pre}})gl$, where m_r is the mass read from the digital scale, m_{pre} is the mass of pre-load, $g$is the gravitational acceleration, and l is the length between the end of the beam and the rotor shaft.

The self-torque can be measured by supplying one single phase with a dc current. For example, 2 A dc current is supplied to phase A, and the self-torque T_a can be obtained as shown in Fig. 19. To measure the mutual torque, first, the same level of dc current (2 A) is supplied to two phases connected in series, e.g., phases A and B, the resultant torque ($T_a+T_b+T_{ab}$) can be measured for different rotor positions. Then, the mutual torque (T_{ab}) can be easily obtained by subtracting self-torque of phases A and B, i.e., T_a and T_b, and the results are shown in Fig. 20. It shows that both DL and SL machines have similar level of mutual torque. It is worth mentioning that the slight discrepancy between measured and FEA results is probably due to the fact that the end windings have not been considered in the FEA simulations.

C. Static Torque

In this section, machines are tested under a pseudosine wave current condition ($I_A = I, I_B = I/2, I_C = -I/2$,

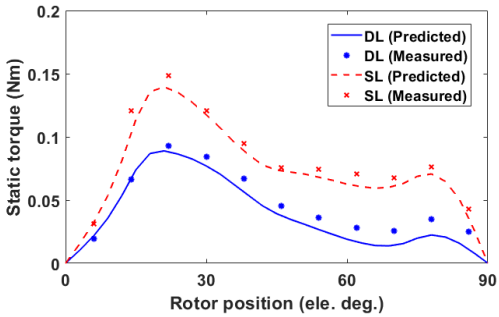

Fig. 21. FEA and measured static torques versus rotor position at 2 A phase rms current for 12s/8p six-phase DS-SRMs.

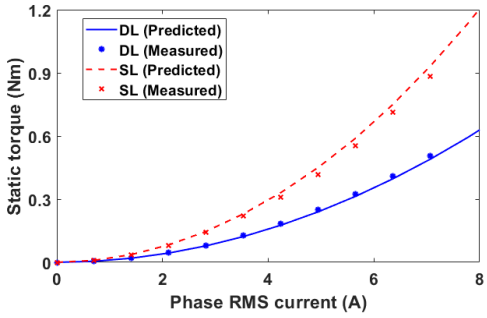

Fig. 22. FEA and measured static torques versus phase rms current for 12s/8p six-phase DS-SRMs.

$I_D = -I, I_E = -I/2$, and $I_F = I/2$), where I is the dc current which is 2.83 A (2 A rms). The static torque at each rotor position (equivalent to current phase advance angle) can be measured as shown in Fig. 21.

After rotor is locked at the position where the maximum average torque can be achieved (phase advance angle of 45° for synchronous reluctance machines), the static torque against phase rms current can be measured and compared with FEA results, as shown in Fig. 22. Overall, a good agreement can be observed between the predicted and measured results.

D. On-Load Static Torque

In order to measure on-load static torque versus rotor positions for six-phase DS-SRMs under sine wave excitation, at least four current generators are required if using the same measurement methods as in Section V-C. This is very inconvenient. However, it is much easier to use two three-phase half-bridge inverters to control the six-phase currents. During the test, the rotors are locked at different rotor positions. At each rotor position, six-phase dc currents are supplied to the machines, and the amplitudes of these currents are chosen according to the values of six-phase sine wave currents at different rotor positions. The torque can then be measured by torque transducer. It is worth noting that, due to the inaccuracy of the torque transducer, higher phase rms current (5 A) has been chosen in this test in order to improve the signal-to-noise ratio. Fig. 23 shows the predicted and measured on-load torques.

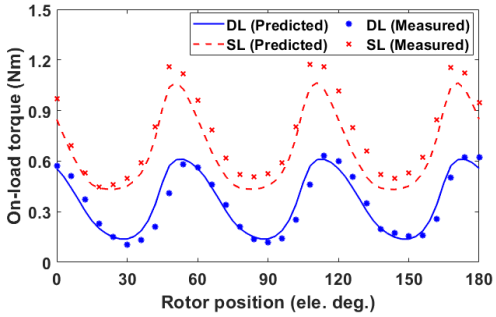

Fig. 23. FEA and measured on-load static torques for 12s/8p six-phase DS-SRMs versus rotor position at 5 A phase rms current.

VI. Conclusion

This paper proposes general instantaneous torque prediction methods for multiphase DS-SRMs. The torque produced by each inductance harmonic can be accurately predicted. Based on the analytical torque equation, it is found that for the DS-SRMs, the torque harmonic frequency only depends on the phase number. Generally, there will be mkth-order torque harmonics for m-phase machine if $\mathrm{mod}(mk, 2) = 0$ is valid, and they are due to the interaction between the fundamental current and the mkth, $(mk \pm 2)$th-order inductance harmonics. However, there is also a special case such as the 12s/10p DL six-phase machines which have self- and mutual- sixth-order torque harmonics canceled one another and inherently lead to much lower torque ripple.

Moreover, it is also found that the second- and four-phase machines will produce inherently higher torque ripple due to the fact that all the inductance harmonics contribute to torque ripple. However, for the five-phase machines, only certain inductance harmonics contribute to torque ripple. Other inductance harmonics, particularly some low-order inductance harmonics ($n < 8$), with relative higher magnitudes, have no influence on torque ripple. As a result, the five-phase machines generally achieve lower torque ripple than other phase numbers. Two prototype six-phase machines with both SL and DL windings have been used for the experimental validations.

References

[1] C. Gan, J. Wu, Q. Sun, W. Kong, H. Li, and Y. Hu, "A review on machine topologies and control techniques for low-noise switched reluctance motors in electric vehicle applications," *IEEE Access*, vol. 6, pp. 31430–31443, 2018.

[2] X. Deng, B. Mecrow, H. Wu, and R. Martin, "Design and development of low torque ripple variable-speed drive system with six-phase switched reluctance motors," *IEEE Trans. Energy Convers.*, vol. 33, no. 1, pp. 420–429, Mar. 2018.

[3] D. H. Lee, T. H. Pham, and J. W. Ahn, "Design and operation characteristics of four-two pole high-speed SRM for torque ripple reduction," *IEEE Trans. Ind. Electron.*, vol. 60, no. 9, pp. 3637–3643, Sep. 2013.

[4] L. R. Huang, J. H. Feng, S. Y. Guo, Y. F. Li, J. X. Shi, and Z. Q. Zhu, "Rotor shaping method for torque ripple mitigation in variable flux reluctance machines," *IEEE Trans. Energy Convers.*, vol. 33, no. 3, pp. 1579–1589, Sep. 2018.

[5] G. J. Li, X. Y. Ma, G. W. Jewell, and Z. Q. Zhu, "Novel modular switched reluctance machines for performance improvement," *IEEE Trans. Energy Convers.*, vol. 33, no. 3, pp. 1255–1265, Sep. 2018.

[6] Q. Ze, D. Liang, P. Kou, and Z. Liang, "Reduction of torque and voltage ripple in a doubly salient permanent magnet generator," *IEEE Trans. Energy Convers.*, vol. 33, no. 2, pp. 702–715, Jun. 2018.

[7] C. Lai, G. Feng, K. Mukherjee, V. Loukanov, and N. C. Kar, "Torque ripple modeling and minimization for interior PMSM considering magnetic saturation," *IEEE Trans. Power Electron.*, vol. 33, no. 3, pp. 2417–2429, Mar. 2018.

[8] L. Parsa, "On advantages of multi-phase machines," in *Proc. 31st Annu. Conf. IEEE Ind. Electron. Soc. (IECON)*, Nov. 2005, p. 6.

[9] X. Deng, B. Mecrow, R. Martin, and S. Gadoue, "Effects of winding connection on performance of a six-phase switched reluctance machine," *IEEE Trans. Energy Convers.*, vol. 33, no. 1, pp. 166–178, Mar. 2018.

[10] G. J. Li, J. Ojeda, E. Hoang, M. Lecrivain, and M. Gabsi, "Comparative studies between classical and mutually coupled switched reluctance motors using thermal-electromagnetic analysis for driving cycles," *IEEE Trans. Magn.*, vol. 47, no. 4, pp. 839–847, Apr. 2011.

[11] X. Liu, Z. Q. Zhu, M. Hasegawa, A. Pride, and R. Deodhar, "Investigation of pwms on vibration and noise in SRM with sinusoidal bipolar excitation," in *Proc. IEEE Int. Symp. Ind. Electron.*, May 2012, pp. 674–679.

[12] X. Liang, G. Li, J. Ojeda, M. Gabsi, and Z. Ren, "Comparative study of classical and mutually coupled switched reluctance motors using multiphysics finite-element modeling," *IEEE Trans. Ind. Electron.*, vol. 61, no. 9, pp. 5066–5074, Sep. 2014.

[13] C. M. Spargo, B. C. Mecrow, J. D. Widmer, and C. Morton, "Application of fractional-slot concentrated windings to synchronous reluctance motors," *IEEE Trans. Ind. Appl.*, vol. 51, no. 2, pp. 1446–1455, Mar/Apr. 2015.

[14] C. M. Spargo, B. C. Mecrow, J. D. Widmer, C. Morton, and N. J. Baker, "Design and validation of a synchronous reluctance motor with single tooth windings," *IEEE Trans. Energy Convers.*, vol. 30, no. 2, pp. 795–805, Jun. 2015.

[15] C. M. Donaghy-Spargo, B. C. Mecrow, and J. D. Widmer, "On the influence of increased stator leakage inductance in single-tooth wound synchronous reluctance motors," *IEEE Trans. Ind. Electron.*, vol. 65, no. 6, pp. 4475–4482, Jun. 2018.

[16] D. Zarko, D. Ban, and T. A. Lipo, "Analytical solution for electromagnetic torque in surface permanent-magnet motors using conformal mapping," *IEEE Trans. Magn.*, vol. 45, no. 7, pp. 2943–2954, Jul. 2009.

[17] B. Gaussens *et al.*, "Magnetic field solution in doubly slotted airgap of conventional and alternate field-excited switched-flux topologies," *IEEE Trans. Magn.*, vol. 49, no. 9, pp. 5083–5096, Sep. 2013.

[18] S. Jia, R. Qu, J. Li, and D. Li, "Principles of stator DC winding excited vernier reluctance machines," *IEEE Trans. Energy Convers.*, vol. 31, no. 3, pp. 935–946, Sep. 2016.

[19] X. Wang, Q. Li, S. Wang, and Q. Li, "Analytical calculation of air-gap magnetic field distribution and instantaneous characteristics of brushless DC motors," *IEEE Trans. Energy Convers.*, vol. 18, no. 3, pp. 424–432, Sep. 2003.

[20] L. R. Huang, J. H. Feng, S. Y. Guo, J. X. Shi, W. Q. Chu, and Z. Q. Zhu, "Analysis of torque production in variable flux reluctance machines," *IEEE Trans. Energy Convers.*, vol. 32, no. 4, pp. 1297–1308, Dec. 2017.

[21] N. Bianchi, S. Bolognani, D. Bon, and M. D. Pré, "Torque harmonic compensation in a synchronous reluctance motor," *IEEE Trans. Energy Convers.*, vol. 23, no. 2, pp. 466–473, Jun. 2008.

[22] T. A. Lopo, *Analysis of Synchronous Machines*, 2nd ed. Boca Raton, FL, USA: CRC Press, 2008.

[23] N. Bianchi and M. D. Pre, "Use of the star of slots in designing fractional-slot single-layer synchronous motors," *IEE Proc.-Elect. Power Appl.*, vol. 153, no. 3, pp. 459–466, May 2006.

[24] E. Fornasiero, L. Alberti, N. Bianchi, and S. Bolognani, "Considerations on selecting fractional-slot nonoverlapped coil windings," *IEEE Trans. Ind. Appl.*, vol. 49, no. 3, pp. 1316–1324, May/Jun. 2013.

[25] Z. Q. Zhu, B. Lee, L. Huang, and W. Chu, "Contribution of current harmonics to average torque and torque ripple in switched reluctance machines," *IEEE Trans. Magn.*, vol. 53, no. 3, pp. 1–9, Mar. 2017.

[26] X. Y. Ma, G. J. Li, G. W. Jewell, Z. Q. Zhu, and H. L. Zhan, "Performance comparison of doubly salient reluctance machine topologies supplied by sinewave currents," *IEEE Trans. Ind. Electron.*, vol. 63, no. 7, pp. 4086–4096, Jul. 2016.

[27] G. J. Li, X. Y. Ma, G. W. Jewell, Z. Q. Zhu, and P. L. Xu, "Influence of conduction angles on single-layer switched reluctance machines," *IEEE Trans. Mag.*, vol. 52, no. 12, pp. 1–11, Dec. 2016.

[28] Z. Q. Zhu, "A simple method for measuring cogging torque in permanent magnet machines," in *Proc. IEEE Power Energy Soc. Gen. Meeting*, Jul. 2009, pp. 1–4.